Saturn's Hydrogen Aurora, WFPC2 Imaging from the Hubble Space Telescope[1]

John T. Trauger[2], John T. Clarke[3], Gilda E. Ballester[3], Robin W. Evans[2], Christopher J. Burrows[4], David Crisp[2], John S. Gallagher III[5], Richard E. Griffiths[6], J. Jeff Hester[7], John G. Hoessel[5], Jon A. Holtzman[8], John E. Krist[4], Jeremy R. Mould[9], Raghvendra Sahai[2], Paul A. Scowen[7], Karl R. Stapelfeldt[2], and Alan M. Watson[6]

(1) Based on observations with the NASA/ESA Hubble Space Telescope;

(2) Jet Propulsion Laboratory, 4800 Oak Grove Drive, Pasadena, CA 91109;

(3) Space Physics Research Laboratory, University of Michigan, 2455 Hayward, Ann Arbor, MI 48109;

(4) Space Telescope Science Institute, 3700 San Martin Drive, Baltimore, MD 21218;

(5) Department of Astronomy, University of Wisconsin – Madison, 475 N. Charter St., Madison, WI 53706;

(6) Department of Physics, Carnegie Mellon University, 5000 Forbes Ave., Pittsburgh, PA 15213;

(7) Department of Physics and Astronomy, Arizona State University, Tyler Mall, Tempe, AZ 85287;

(8) Department of Astronomy, New Mexico State University, Las Cruces, NM 88003;

(9) Mount Stromlo and Siding Springs Observatories, Weston Creek, A.C.T. 2611, Australia.

ABSTRACT

WFPC2/HST images of Saturn's far-ultraviolet aurora reveal emissions confined to a narrow band of latitudes near Saturn's north and south poles. The aurorae are most prominent in the morning sector with patterns that appear fixed in local time. The geographic distribution and vertical extent of the auroral emissions seen in these images provide the first new observational insights into the physical mechanisms that power Saturn's aurora since the Voyager encounters seventeen years ago.

INTRODUCTION

Saturn's far-ultraviolet aurora was first observed just seventeen years ago by Pioneer 11, and has since been observed by the International Ultraviolet Explorer (IUE), Voyager Ultraviolet Spectrometer (UVS), and most recently by the Hubble Space Telescope spectrographs and cameras. We have known, since the Voyager encounters in 1980 and 1981, that Saturn's auroral emissions are variable and the physical mechanisms that power them must involve both internal sources and solar wind interactions.

Auroral emissions were first observed from Saturn as polar limb brightenings by the Pioneer 11 long wave photometer (Judge et al., 1980), and as time variable H Lyα emissions from Saturn's polar regions by IUE (Clarke et al. 1981). Longer term IUE observations showed that emissions were detected only sporadically from the brightest Saturn auroral events (McGrath and Clarke, 1992). Polar auroral emissions were unambiguously identified on Saturn by the Voyager UVS (Broadfoot et al., 1981). The UVS observed an auroral emission source confined between -78° and -81.5° south latitude as Voyager 1 passed over Saturn's south pole (Sandel and Broadfoot, 1981). The Voyager 1 UVS monitored the north and south auroral emissions for a few Saturn rotations before and after encounter, finding variable auroral emissions which peaked in intensity when the sub-solar meridian passed through $\sim$ 115° Saturn Longitude System (SLS) (Sandel et al., 1982). The UVS on Voyager 2 fixed its field of view at about 80° north latitude and 0900 local time (LT) for a full Saturn rotation prior to encounter, again finding auroral emissions and significant auroral brightening when the sub-solar SLS was near 115°. The UVS auroral emission spectra were shown to be consistent with electron collisional excitation of molecular hydrogen (Shemansky and Ajello, 1983). However, neither Voyager encounter provided sufficient coverage to discriminate between temporal, longitudinal, or LT variations in the auroral morphology.

Voyager spacecraft observed radio emissions that were strongly correlated with both sub-solar longitude (Gurnett et al., 1981) and variations in the solar wind pressure at Saturn (Desch, 1982). The auroral brightenings at sub-solar SLS near 115° correlated well with the geometry for most probable Saturn kilometric radiation (SKR) (Kaiser et al., 1984). During its passage near Saturn's south pole, Voyager 1 magnetometers detected the magnetic signature of an inflowing $\sim 10^7$ ampere field-aligned current at a LT of 2130. This was modeled in terms of a current system driven by a solar wind dynamo, flowing inward along field lines at dusk as observed, then inferred to flow through the ionosphere across the polar cap and exit (i.e. auroral electrons inflowing) along field lines in the morning sector (Connerney et al., 1983). In addition, the Voyager magnetometer experiments were used to constrain a preliminary axisymmetric magnetic field model, which together with measurements of the magnetic field strength and dimensions of Saturn's magnetotail was used to predict that the auroral latitudes would fall between 75° and 79° north and south based on conservation of magnetic flux (Ness et al., 1981), thus making an association between the location of auroral emissions and the boundaries of the magnetopause. More recent estimates (J.E.P. Connerney, personal communication, 1995) based on conservation of magnetic flux and the Z3 magnetic field model (Connerney et al., 1982) map the magnetopause to predicted auroral zones at 77.3° to 80.5° north and -76.1° to -79.5° south. Observations of Saturn near-IR H_3^+ emissions have revealed only very faint emission from the aurora, although the same technique found bright emission from Jupiter's aurora and emissions from Uranus (Geballe et al., 1993).

Saturn's aurora has been associated with dark polar absorption caps, seen with greatest contrast at shorter UV wavelengths, and also with less contrast in the visible (West et al., 1983; Pryor and Hord, 1991; Karkoschka and Tomasko, 1993; Ben Jaffel et al., 1995; Gérard et al., 1995). The dark polar caps are due to stratospheric aerosols produced above the 10 mBar level that are distinctly smaller ($\sim 0.15\mu$m) than typical tropospheric aerosols

($\sim 1.5\mu$m), and may be produced directly from the stratospheric gases (Karkoschka and Tomasko, 1993). Since the polar caps underlie the auroral regions, these aerosols are likely to be the products of auroral chemistry.

Saturn's magnetic field and magnetosphere present a case that is intermediate between the solar-wind dominated conditions at the Earth and the more complex conditions at Jupiter. The Earth's magnetosphere draws most of its energy from the solar wind, and the Earth's aurora is fixed in LT. Jupiter's magnetic field has an order of magnitude greater surface field strength, and the dominant auroral morphologies tend to corotate with the planet. Jovian nonthermal radio emissions have been observed for nearly 40 years. Jovian decametric radiation exhibits periodicities due to planet rotation and the orbital motion of Io. The Jovian magnetosphere is populated largely by Iogenic sulfur and oxygen ions, and the internal plasma is powered by the acceleration and diffusion of ions as they are swept into corotation with Jupiter. While Saturn is similar in size and composition to Jupiter, its magnetic field is similar in surface strength to the Earth's. Unlike either the Earth or Jupiter, Saturn's magnetic field is very closely aligned with the rotation axis. Saturn has internal sources of plasma from its rings, icy satellites, and Titan, but the relative importance of these internal sources is thought to be less than at Jupiter.

Here we report far-ultraviolet observations of Saturn's aurora obtained in October 1994 and 1995 with the WFPC2 camera on board the Hubble Space Telescope. A physical model is used to unfold the planetocentric distribution of the aurora from the observed aurora morphology. Auroral emissions are modeled as a chapman profile illuminating the magnetic field lines passing through discrete planetocentric "footprints," leading to a determination of the location of the emissions and the associated radiated power. The intensities of the observed aurorae are significantly variable on the shortest time scales measured. The location of the brightest emissions appears to be stationary in local time,

suggesting an excitation mechanism that is dominated by interactions between the solar wind and planetary magnetosphere.

OBSERVATIONS

We report WFPC2 images of Saturn's aurora taken with far-ultraviolet (FUV) filter combinations that include the emission lines of H_2 (Lyman and Werner bands shortward of 1650Å), atomic hydrogen Lyα emission at 1216Å, and the Rayleigh-scattered solar continuum (mostly longward of 1800Å). The entire planet and rings were imaged in one of WFPC2's four cameras, the WF3 camera with pixel dimensions of 0.1 arcsec (about 750 km at Saturn's distance). All observations utilized the Wood's filter F160WB, a broad photometric filter covering the 1200-2100Å wavelength range. The Wood's filter is unique to the WFPC2 instrument, using a thin layer of metallic sodium to provide a broad far-ultraviolet passband while strongly attenuating all radiation longward of the sharp 2100 Å cutoff. Exposures were made either with the Wood's filter alone, or with the Wood's filter crossed with a short-wavelength blocking filter to distinguish between auroral emissions and the rayleigh-scattered solar continuum. The blocking filters F130LP and F165LP were used to eliminate wavelengths shortward of 1300 and 1650Å respectively.

Photometry in the wide F160WB filter passband is hampered by a lack of direct measurement of the spectral structure in the auroral emissions and atmospheric absorptions across the passband, and still further limited by uncertainties in the WFPC2 calibration at FUV wavelengths. Fortunately we can draw on comparisons with the better-studied case of Jovian aurora, which is expected to have a similar emission spectrum. As for the case of Saturn, HST/GHRS observations of Jupiter's aurora and supporting laboratory work indicate that the FUV emission spectrum is consistent with an optically thin electron-excited H_2 emission spectrum (Clarke et al., 1994; Trafton et al., 1994; Kim et al., 1995).

Based on this comparison, WFPC2's limiting sensitivity in the far-UV is roughly 10 kilo-Rayleighs (kR) per pixel in exposures short enough (~16 minutes) to distinguish between possible corotating and LT-fixed auroral components. (One kR is the apparent surface brightness from a column emission of 10^9 photons/cm^2/sec into 4π stearadians). The 1995 observations also included exposures with the F160WB+F130LP filter combination as a measure of auroral color, and F218W images to define the regions of dark polar haze. Our observations of Saturn show peak auroral surface brightnesses a factor of ~30 fainter than the brightest emissions in Jupiter's aurora (Ballester et al., 1996; Clarke et al., 1996).

Our Saturn viewing geometry and other details of the exposures are summarized in Table 1. The Earth was 7.8° north of Saturn's equatorial plane in October 1994, providing our best views of Saturn's north polar aurora. The Earth was near 2° north in October 1995, giving roughly equal access to both north and south polar regions. We list the JPL Ephemeris value for Saturn's central meridian longitude for reference. The position angle in the sky of the WFPC2 field of view and the observing time are HST engineering data taken from the STScI data headers. These are input to JPL's NAIF software package and database (Acton, 1996) in order to locate latitudes, longitudes, and the limb outline at the 1-bar reference surface. The planet center, the only fitted parameter in the navigation process, is estimated by matching the geometrically-corrected WFPC2 images to the ephemeris-predicted limb outlines. The accuracy of the predicted limb outline is determined by the accuracy of our knowledge of WFPC2's plate scale (0.03%), the distance to Saturn (0.0001%), and the dimensions taken for the 1-bar reference spheroid (60268 and 54364 km respectively for the equatorial and polar radii). Therefore, the projected limb outline should be scaled correctly to within about 20 km. We estimate that the centering of the limb outline on the planet image, on the other hand, is accurate to about ±0.25 of a pixel, or about ±200 km when projected to the planet surface, due to uncertainties in determining the limb boundaries in the data. This ±200 km positioning uncertainty is

therefore the dominant error in locating the planet's reference surface.

As intended, SLS 115° appears within ±30° of Saturn's noon meridian in all three observing sequences. This provides three independent observations of the same longitude range. But we also note that Saturn's rotation period is sufficiently uncertain that it is not possible to infer valid correlations between the Voyager-epoch longitudes associated with peaks in auroral and SKR emissions and current-epoch observations of aurora activity (M. Kaiser, personal communication, 1997). With a Voyager-determined Saturn rotation period of $10^h39^m24^s \pm 7^s$ (Desch and Kaiser, 1981), the accumulated uncertainty between current Saturn longitudes and SLS since the Voyager epoch is roughly ±2 Saturn rotations.

Figure 1 illustrates the FUV appearance of Saturn as obtained by summing the four F160WB images taken on 9 October 1994. An image taken in F160WB+F165LP at the outset of the observing sequence (not shown here) demonstrates that Saturn's disk, dark polar regions, and its rings are seen in reflected solar light longward of 1650 Å, while the polar auroral emissions are seen only at wavelengths shortward of 1650 Å. Since this is a summation over ~80° of rotation, the image emphasizes the prominent north polar auroral feature which appeared fixed in LT near the dawn limb. To illustrate the development of the auroral feature over our short 1994 observing sequence, a magnified view of the north polar regions in the four exposures taken with the F160WB filter is shown in Figure 2. The bright auroral feature appears in strong contrast to the dark polar atmospheric background, with peak intensities comparable to and sometimes brighter than the planet disk as seen in the F160WB passband. Significant intensity variations on time scales of ~16 minutes are evident in the 1994 data. Figure 2 also includes the single F160WB images taken on 15 and 31 October 1995, the first showing no detectable auroral emissions, while the second shows fainter emissions confined between dawn and noon LT, but without the prominent dawn-fixed brightening seen in 1994. The 1995 observations lacked rotational coverage, but

revealed important long-term changes in the auroral morphology. Comparable southern auroral intensities were also observed in the 1995 images, but are not shown in Figure 2. While the aurora seen on our three observing dates yielded three distinct intensity distributions, all of the observed emissions were most prominent in the morning sector.

Dark polar caps are seen in all FUV images reported here, extending from the poles equatorward to about 60° latitude in the north, and to comparable latitudes in the south. The dark FUV cap was first reported as a dark ring centered at ~79° north latitude in 2200 Å deconvolved images with the HST/FOC (Ben Jaffel et al., 1995). We see no evidence for a comparable ring structure in our images. Images taken with the F160WB+F165LP filter combination that excludes all FUV auroral emissions, as well as the F218M images with wavelength coverage comparable to the FOC observations reveal polar caps that are dark with no significant emissions anywhere poleward of ~60°. Since we attribute the dark polar caps to fine haze particles created high in the stratosphere in direct response to auroral activity, it may be possible that the caps are diminished to rings if observed during periods of reduced auroral activity. It is also possible that the reported ring structure is a false processing artifact generated during image deconvolution near the dark limbs of the planet in the FOC images. The polar caps extend significantly equatorward of the latitudes of auroral activity in all WFPC2 images reported here, evidence of latitudinal transport of haze aerosols in the upper atmosphere.

ANALYSIS

The images have been processed to account for known WFPC2 instrument characteristics. Image reduction includes intensity calibration, flat-field and dark noise corrections, removal of proton and cosmic ray events, and a small correction for optical geometric distortion. These are detailed with further references in a number of publications, including

Koratker and C. Leitherer (1996) and Biretta (1996). The Saturn observations followed the last previous thermal maintenance cycle of the WFPC2 CCDs by 14, 23, and 14 days respectively in the 9 October 1994, 15 October 1995, and 31 October 1995 observations. Limiting sensitivities were roughly 10 kR per pixel in F160WB, F160WB+F130LP, and F160WB+F165LP exposures used to isolate atomic hydrogen Lyα and H_2 Lyman and Werner band emissions. These Saturn auroral intensity estimates are based on expected similarities with the Jovian auroral spectrum, which has been studied with WFPC2, the HST/GHRS, and IUE. The GHRS and IUE spectrographs are photometrically calibrated in the FUV, providing a rough intensity calibration of the combination of all auroral atomic and molecular emission lines shortward of 1650Å, as detected with WFPC2's FUV filter combinations.

We describe the salient features of these emissions, including their latitude confinement, vertical extent, time variations, and systematic longitudinal characteristics. Near the dawn and dusk limbs, the latitude and base altitude of the polar auroral emissions are easily measured due to the viewing angle, while the longitudes of the emissions are difficult to determine. On the other hand, near the central longitudes it is longitude structure that is easily measured, while it is difficult to distinguish between latitude and base altitudes. The location of the auroral emissions observed in 1994, when the observing sequence was long enough to detect longitudinal motions that could be correlated with orbiting satellites, showed no direct correspondence with the location or movement of the magnetic footprints of any of Saturn's satellites. An initial indication of the vertical extent of the aurora is apparent from the imagery, with features that appear to extend at least 2000 km beyond the polar limbs in 1994 images.

An aurora model is required for a more precise location of the source of auroral emissions within our viewing geometry. The Z3 magnetic field model (Connerney, 1993) is used to

trace magnetic field lines originating at the 1-bar reference surface within specific ranges of planetocentric longitude and latitude. The aurora model is built up from individual magnetic field lines, each illuminated with an emission intensity $I(h)$ given by a Chapman production profile, as follows. From a point of origin (latitude and longitude) on the 1-bar reference surface, each field line passes vertically from an atmospheric height h_0 to a maximum height h_m that is sufficiently high that auroral emissions are insignificant. The atmospheric scale heights are H_0 for $h_0 \leq h < h_1$, then H_1 for $h_1 \leq h < h_m$. The corresponding Chapman profile generates one or two peaks in the emission intensities along the illuminated field line, as determined by the excitation cross sections and atmospheric density profile. In this case, we select $h = h_{peak}$ within the range $h_1 < h_{peak} < h_m$, and a second peak appears at the foot of the illuminated field line just below h_1. The intensity $I(h)$ at a height h along the field line is given by:

$$I(h) = I_1 exp\left[\left(\frac{h_1 - h}{H_1}\right) - a_1 exp\left(\frac{h_1 - h_m}{H_1}\right)\left[exp\left(\frac{h_m - h}{H_1}\right) - 1\right]\right]$$

for $h_1 \leq h < h_m$, and

$$I(h) = I_0 exp\left[\left(\frac{h_0 - h}{H_0}\right) - a_0 exp\left(\frac{h_0 - h_m}{H_0}\right)\left[exp\left(\frac{h_m - h}{H_0}\right) - exp\left(\frac{h_m - h_1}{H_0}\right)\right]\right]$$

for $h_0 \leq h < h_1$, where

$$a_1 = exp\left(\frac{h_{peak} - h_1}{H_1}\right), a_0 = \frac{H_0}{H_1} exp\left(\frac{h_1 - h_0}{H_0}\right) exp\left(\frac{h_{peak} - h_1}{H_1}\right), and$$

$$I_0 = I_1 exp\left(\frac{h_1 - h_0}{H_0}\right) exp\left[exp\left(\frac{h_{peak} - h_1}{H_1}\right)\left[exp\left(\frac{h_1 - h_m}{H_1}\right) - 1\right]\right]$$

We have fixed the base of auroral emissions on the assumption that methane absorption shortward of 1450 Å will strongly attenuate auroral emissions from source regions below the homopause, which we take to be 1000 km above the 1-bar reference level (Smith et al., 1983). Hence the three parameters to be determined by comparison with Saturn aurora images are H_1, I_1, and h_{peak} for each point of origin on the Saturn reference surface. In the present work, H_1 and h_{peak} have been considered constants over the entire data set.

With the reasonable assumption that electron-excitation of molecular hydrogen is the predominant source of Saturn's auroral emissions (Shemansky and Ajello, 1983), the H_2 atmospheric scale heights are appropriate for the dominant target species. We adopt for the target atmosphere the molecular hydrogen scale height of $H_0 = 64$ km up to $h_1 = 1000$ km above the 1-bar level (Festou and Atreya, 1982), and a larger (model-determined) scale height H_1 above 1000 km. We zero out all emissions from below ~900 km due to methane attenuation below the homopause. Our Chapman model is based on a simple mechanism for conversion of the energy of precipitating particles into observable FUV emissions. We have assumed a deposition of particle energy with a fixed effective cross section. The atmospheric scale height H_1 above 1000 km and the effective cross section for excitation were adjusted to give a Chapman model which best fit the six aurora images illustrated in Figure 2.

Auroral intensities I_1 were computed for each image in terms of individual bundles of Chapman-illuminated field lines, each originating from 256 discrete rectangular areas on the reference 1-bar surface, each dimensioned 1° in latitude by 1-hour in LT (15° in longitude). These 256 individual model components were convolved with a representative point spread function (PSF) derived from a calibration exposure (u2a71i0gt3) of a star taken in WFPC2's F170W filter on 20 October 1994. The planetocentric distribution of auroral emissions was determined by least-squares fitting of these 256 individual components to

the auroral image using model "footprints" that covered $4-18$ hours in LT and $66°-82°$ in latitude. The representative fitted model is shown in Figure 3, where it is compared to the WFPC2 aurora image. The radiated power associated with these fitted auroral components is mapped against north latitude and LT in Figure 4. WFPC2-observed northern auroral emissions are confined mostly between the latitudes of 74° and 79°. In all four of the 1994 images, the auroral components were strongly peaked between 75° and 77° in latitude and 7 to 9 hours in LT. Similar but less well-constrained latitudes were observed in the south. While placing unambiguous latitude and longitude constraints on the auroral source regions, the model does not strongly constrain the vertical distribution of the emissions. Here we have adopted a best-fit model scale height of 750(±300) km for the atmosphere above the homopause, and a peak-emission altitude near the homopause (1000 ± 300 km).

The brightest observed emissions (the brightest pixel in 1994 data is found in image u21q0103) reached $\sim$ 94 kR, while the threshold for detection of auroral emissions averaged over 15° in longitude is about 5 kR. Integrating the northern auroral emissions in this image yields a total FUV radiated power of about 4×10^{10} Watts. These peak values are to be compared with the Jovian aurorae as observed with WFPC2, in which radiated power ranges typically from a few $\times 10^{11}$ to 10^{12} Watts integrated over the Jovian northern auroral oval, with intensities ranging typically from 300 to 3000 kRay (Clarke et al. 1996).

DISCUSSION

The peak observed Saturn auroral surface brightnesses are more than an order of magnitude fainter than the brightest emissions in Jupiter's aurora, with total radiated power observed to vary between a few $\times 10^{10}$ Watts to below the observational threshold of about 10^8 Watts. Within the limited time coverage of these observations, the brightest auroral features are

typically seen in the dawn-to-noon sector. The brightest aurora observed in 1994 appeared to be fixed in LT. The latitude confinement of the auroral zones is in good agreement with Voyager experiments referenced earlier.

These WFPC2 results are to be compared with the Voyager radio observations of SKR, which identified radio source regions also apparently fixed in LT. A physical relationship is expected between Saturn's auroral activity and SKR, since they are both associated with the precipitation of electrons into Saturn's upper atmosphere, and because Voyager experiments found a correlation between intensity of Saturn's auroral emissions and the probability of detecting SKR. Voyager also found a correlation between the level of SKR activity and solar wind dynamic pressure at Saturn, hence interactions between Saturn's magnetosphere and the solar wind are implicated in the production of SKR. Independent analyses of the Voyager radio data (Kaiser and Desch, 1982; Lecacheux and Genova, 1983; Galopeau et al., 1995) have produced a number of inferred SKR source regions. The most recent of these refines earlier work and suggests that the SKR emissions radiate predominantly from magnetically conjugate source regions somewhere within boundaries defined by latitudes above $\sim$80° at mid-day LT, and extending to latitudes as low as 60° near dawn (0800-0900 LT) and to 75° near dusk (1900 LT). Our direct images of Saturn's aurora localize the emission regions well within the Voyager-observed SKR boundaries. Because our data set is small, it has not been possible to investigate the Voyager-observed correlation between auroral (and SKR) emission intensities and the sub-solar passage of a small range of Saturn longitudes near 115° SLS during the Voyager epoch, and to gain further insight into an inferred but unobserved anomaly in Saturn's axisymmetric magnetic field. However, it may be possible to correlate our observed variations in auroral activity with contemporaneous SKR observations in 1994-5 by the Ulysses spacecraft (A. Lecacheux, personal communication, 1997).

These features indicate that solar wind interactions play an important role in the auroral morphology. The corotating plasma, bounded by the magnetopause, is forced to flow outward on the evening side of Saturn, then inward on the morning side, creating charged particle acceleration mechanisms that are spatially locked in local time. A general discussion of particle acceleration mechanisms for the analogous case of the Jovian magnetosphere is found in Hill et al. (1983). The location of the dawn-fixed auroral features is also consistent with suppositions that MHD waves driven by Kelvin-Helmholtz instabilities at the magnetopause (Galopeau et al., 1995) or by centrifugal flute instabilities at the outer edge of the dayside plasmasheet (Curtis et al., 1986) play an important role in powering and shaping Saturn's auroral features. The K-H mechanism leads to LT-fixed features that favor the morning sector due to the dependence of its instability threshold on the relative velocities of the impinging solar wind plasma and the corotating magnetospheric plasma, which is always greatest on the dawn side. All of these mechanisms provide avenues for the acceleration of magnetospheric electrons along magnetic field lines to keV energies, thus connecting the acceleration mechanisms along magnetic field lines to the auroral zones. Other mechanisms have been proposed for the acceleration of auroral electrons, including wave-particle interactions in the tenuous plasma torus associated with Titan, generating low-energy electrons and powered essentially by planetary rotation rather than solar wind interactions (Barbosa, 1987 and 1990). As proposed, the torus mechanism would produce an aurora that is more or less uniform in longitude near the observed auroral latitudes. A uniform auroral band is not seen in our images, suggesting that auroral contributions from this mechanism must be significantly fainter than the observed aurora and below our detection threshold.

We may compare these results with independent observations taken with the HST/FOC/COSTAR on 2 October 1994 (Gérard et al., 1995), one week prior to our 1994 WFPC2 observations. FOC provides less sensitivity than WFPC2 for auroral emissions observed with FOC's

F152M+F175W filter combination, therefore eight individual exposures (8400 seconds in total) covering a 13-hour observing period (one complete Saturn rotation) were coadded to produce an auroral detection which is presented in an enhanced-contrast image. About seven auroral spots are reported near 80° north latitude. The implied result is that the FOC observed an aurora distributed over all longitudes near 80° north latitude, but no information is available on the time development of auroral features or the question of LT-fixed vs. planet-fixed phenomena. As evidenced by the difference between the individual WFPC2 F160WB exposures taken two weeks apart in October 1995, there is no reason to expect that bright features in the Saturn aurora remained constant over the one week period separating the FOC and WFPC2 observations in 1994.

Future imaging observations that include a statistically significant sample of complete Saturn rotations spaced apart by weeks to months will be required to distinguish between candidate auroral excitation mechanisms and to further investigate the Voyager observed correlations between sub-solar longitudes and peak auroral emissions. Observations with present and future HST instruments could help resolve these questions.

This work is based on observations with the NASA/ESA Hubble Space Telescope, obtained at the Space Telescope Science Institute, which is operated by AURA Inc. for NASA under contract NAS5-26555. This research was supported by NASA contract NAS7-1260 to the Jet Propulsion Laboratory.

REFERENCES

Acton, C.H., Ancillary Data Services of the NASA Navigation and Ancillary Information Facility, *Planet Space Sci. 44*, 65, 1996.

Ballester, G.E., et al., Time-Resolved Observations of Jupiter's Far-Ultraviolet Aurora, *Science 274*, 409, 1996.

Barbosa, D.D., Titan's Atomic Nitrogen Torus: Inferred Properties and Consequences for the Saturn Aurora, *Icarus 72*, 53, 1987.

Barbosa, D.D., Auroral Precipitation Flux of Ions and Electrons in Saturn's Outer Magnetosphere, *Planet Space Sci. 38*, 1295, 1990.

Ben Jaffel, L., V. Leers, and B.R. Sandel, Dark Auroral Oval on Saturn Discovered in Hubble Space Telescope Ultraviolet Images, *Science 269*, 951, 1995.

Biretta, J. (Ed.), *WFPC2 User's Handbook, Version 4.0*, Space Telescope Science Institute, 1996.

Broadfoot, A.L. et al., Extreme Ultraviolet Observations from Voyager 1 Encounter with Saturn, *Science 212*, 206, 1981.

Clarke, J.T., H.W. Moos, S.K. Atreya, and A.L. Lane, IUE Detection of of Bursts of H Ly α Emission from Saturn, *Nature, 290*, 226, 1981.

Clarke, J.T., et al., Hubble Space Telescope Goddard High-Resolution Spectrograph H_2 Rotational Spectra of Jupiter's Aurora, *Ap. J. 430*, L73, 1994.

Clarke, J.T., et al., Far-Ultraviolet Imaging of Jupiter's Aurora and the Io "Footprint," *Science 274*, 404, 1996.

Connerney, J.E.P., N.F. Ness, and M.H. Acuna, Zonal Harmonic Model of Saturn's Magnetic Field from Voyager 1 and 2 Observations, *Nature 298*, 44, 1982.

Connerney, J.E.P., M.H. Acuna, and N.F. Ness, Currents in Saturn's Magnetosphere, *J.*

Geophys. Res. 88, 8779, 1983.

Connerney, J.E.P., Magnetic Fields of the Outer Planets, *J. Geophys. Res. 98*, 18659, 1993.

Curtis, S.A., R.P. Lepping, and E.C. Sittler Jr., The Centrifugal Flute Instability and the Generation of Saturn Kilometric Radiation, *J. Geophys. Res. 91*, 10989, 1986.

Desch, M.D. and M.L. Kaiser, Voyager Measurement of the Rotation Period of Saturn's Magnetic Field, *Geophys. Res. Let. 8*, 253, 1981.

Desch, M.D., Evidence of Solar Wind Control of Saturn Radio Emission, *J. Geophys. Res. 87*, 4549, 1982.

Festou, M.C., and S.K. Atreya, Voyager Ultraviolet Stellar Occultation Measurements of the Composition and Thermal Profiles of the Saturnian Upper Atmosaphere, *Geophys. Res. Lett. 9*, 1147, 1982.

Galopeau, P.H.M., P. Zarka and D. Le Queau, Source Location of SKR: the Kelvin-Helmholtz Instability Hypothesis, *J. Geophys. Res. 100*, 26397, 1995.

Geballe, T.R., M.F. Jagod, and T. Oka, Detection of H_3^+ Infrared Emission Lines in Saturn, *Ap. J. 408*, L109, 1993.

Gérard, J.-C., V. Dols, D. Grodent, J.H. Waite, G.R. Gladstone, and R. Prangé, Simultaneous Observations of the Saturnian Aurora and Polar Haze with the HST/FOC, *J. Geophys. Res. 22*, 2685, 1995.

Gurnett, D.A., W.S. Kurth, and F.L. Scarf, Plasma Waves near Saturn: Initial Results from Voyager 1, *Science 212*, 235, 1981.

Hill, T.W., A.J. Dessler, and C.K. Goertz, Magnetospheric Models, *Physics of the Jovian Magnetosphere*, A.J. Dessler (Ed.), Section 10.6, Cambridge University Press, 1983.

Judge, D.L., F.M. Wu, R.W. Carlson, Ultraviolet Photometer Observations of the Satur-

nian System, *Science, 207*, 431, 1980.

Kaiser, M.L. and M.D. Desch, Saturnian Kilometric Radiation: Source Location, *J. Geophys. Res. 87*, 4555, 1982.

Kaiser, M.L., M.D. Desch, W.S. Kurth, A. Lecacheux, F. Genova, B.M. Pederson, and D.R. Evans, in *Saturn* (University of Arizona Press, 1984), T. Gehrels and M.S. Matthews (eds), 378.

Karkoschka, E. and M.G. Tomasko, Saturn's Upper Atmospheric Hazes Observed by the Hubble Space Telescope, *Icarus 106*, 428, 1993.

Kim, Y.H., J.J. Caldwell, and J.L. Fox, High-Resolution Ultraviolet Spectroscopy of Jupiter Aurora with the Hubble Space Telescope, *Ap. J. 447*, 906, 1995.

Koratker A., and C. Leitherer (Eds.), Proceedings of the HST Calibration Workshop, *Space Telescope Science Institute*, 1996.

Lecacheux, A. and F. Genova, Source Location of Saturn Kilometric Radio Emission, *J. Geophys. Res. 88*, 8993, 1983.

McGrath, M.A. and J.T. Clarke, H I Lyman Alpha Emission from Saturn (1980-1990), *J. Geophys. Res., 97*, 13691, 1992.

Ness, N.F., et al., Magnetic Field Studies by Voyager 1: Preliminary Results at Saturn, *Science 212*, 211, 1981.

Pryor, W.R. and C.W. Hord, A Study of Photopolarimeter System UV Absorption Data on Jupiter, Saturn, Uranus, and Neptune: Implications for Auroral Haze Formation, *Icarus 91*, 161, 1991.

Sandel, B.R. and A.L. Broadfoot, Morphology of Saturn's Aurora, *Nature 292*, 679, 1981.

Sandel, B.R., et al., Extreme Ultraviolet Observations from the Voyager 2 Encounter with Saturn, *Science 215*, 548, 1982.

Shemansky, D.E. and J.M. Ajello, The Saturn Spectrum in the EUV – Electron Excited Hydrogen, *J. Geophys. Res. 88*, 459, 1983.

Smith, G.R., et al., Saturn's Upper Atmosphere from the Voyager 2 EUV Solar and Stellar Occultations, *J. Geophys. Res. 88*, 8667, 1983.

Trafton, L.M., J.-C. Gérard, G. Munhoven, and J.H. Waite, High-Resolution Spectra of Jupiter Northern Auroral Ultraviolet Emission with the Hubble Space Telescope, *Ap. J. 421*, 816, 1994.

West, R.A., et al., Photometry and Polarimetry of Saturn at 2640 and 7500 Å, *J. Geophys. Res. 88*, 8679, 1983.

TABLE 1

Image	UT	CML	LAT	*WFPC2 Passband*	Exposure (sec)
9 October 1994:					
u2iq0101	11:06	41.8°	7.8°	*F673N*	2
u2iq0102	11:26	52.7°	7.8°	*F160BN15+F165LP*	1500
u2iq0103	12:38	93.2°	7.8°	*F160BN15*	1000
u2iq0104	13:01	106.1°	7.8°	*F160BN15*	1000
u2iq0105	14:14	147.2°	7.8°	*F160BN15*	1000
u2iq0106	14:36	159.8°	7.8°	*F160BN15*	800
u2iq0107	14:46	165.6°	7.8°	*F673N*	2
15 October 1995:					
u2wc0101	7:35	116.6°	2.2°	*F218W*	300
u2wc0102	7:57	129.0°	2.2°	*F160BN15*	1500
u2wc0103	9:04	167.1°	2.2°	*F218W*	500
u2wc0104	9:30	181.3°	2.2°	*F160BN15+F130LP*	1500
31 October 1995:					
u2wc0201	17:41	110.4°	2.5°	*F218W*	300
u2wc0202	18:04	123.3°	2.5°	*F160BN15*	1500
u2wc0203	19:09	160.3°	2.5°	*F218W*	500
u2wc0204	19:35	174.6°	2.5°	*F160BN15+F130LP*	1500

Table 1. Summary WFPC2 exposures of the Saturn aurora on three observing dates, including the STScI archival name, universal time (UT), central meridian longitude (CML), planetocentric latitude of the Earth (LAT), filter combination, and exposure time. UT, LAT, and CML are taken at the mid-point of each exposure. Note that Saturn's rotation period is sufficiently uncertain that longitudes estimated in the current epoch have no correspondence to those at the time of the Voyager encounters in 1980-81. They are included only for comparisons among the images presented here.

FIGURE CAPTIONS

Figure 1. Summation of the four F160WB images of Saturn obtained in October 1994. The bright auroral features appear in sharp contrast above a dark stratospheric polar cap.

Figure 2. Six magnified views of Saturn's north polar aurora as observed with the F160WB filter. The development of the aurora in four images numbered 103-106, taken over a two hour period in 1994 during which Saturn rotated 80°, shows prominent auroral features that remained fixed in Saturn local time between dawn and noon. Single exposures obtained on two observing dates in 1995 capture distinctly different auroral morphologies. Graphic overlays locate the planet limb and lines of 75°, 60°, and 45° north latitude, all at the 1-bar reference level in Saturn's atmosphere.

Figure 3. Auroral model fit to the u2iq0103 image (see Table 1). The aurora-only image (a) results from subtracting the continuum-only image numbered 102 from image 103. The auroral model is least-squares fitted to the continuum-subtracted image, resulting in the model aurora shown in (b). The success of the model representation can be inferred from the residual image (c), obtained by subtracting fitted model (b) from aurora image (a).

Figure 4. Plot of the latitude and longitude distribution of radiated power obtained from the model fit to image 103 and shown in Figure 3. The power associated with 256 individual planetocentric auroral "footprints", each dimensioned 1 hour in LT (15° in longitude) by 1° in latitude, ranges from zero (undetectable) to a maximum of 3.0×10^9 Watts as indicated by the color scale at right.

Trauger et al. Figure 1

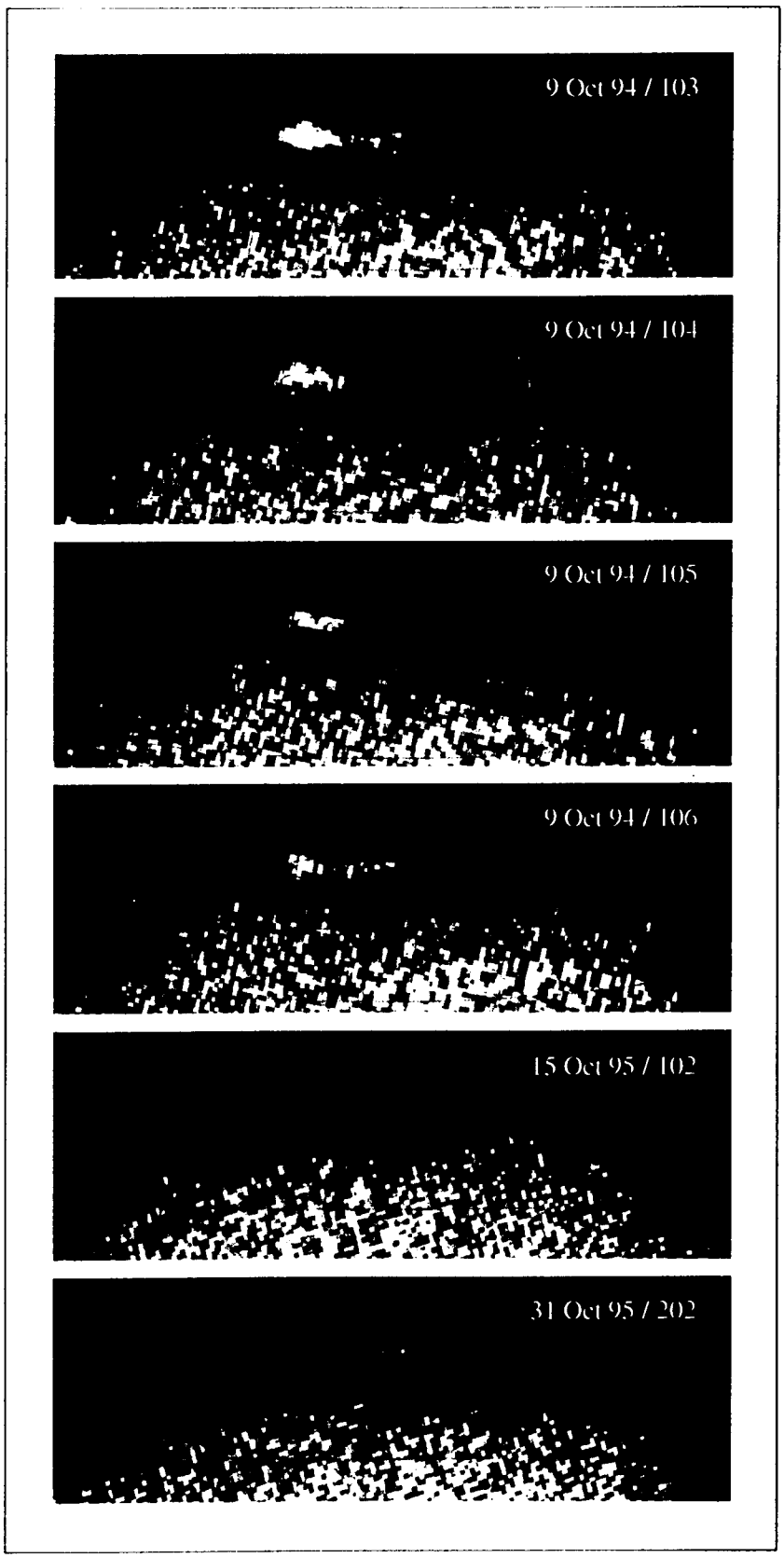

Trauger et al. Figure 2

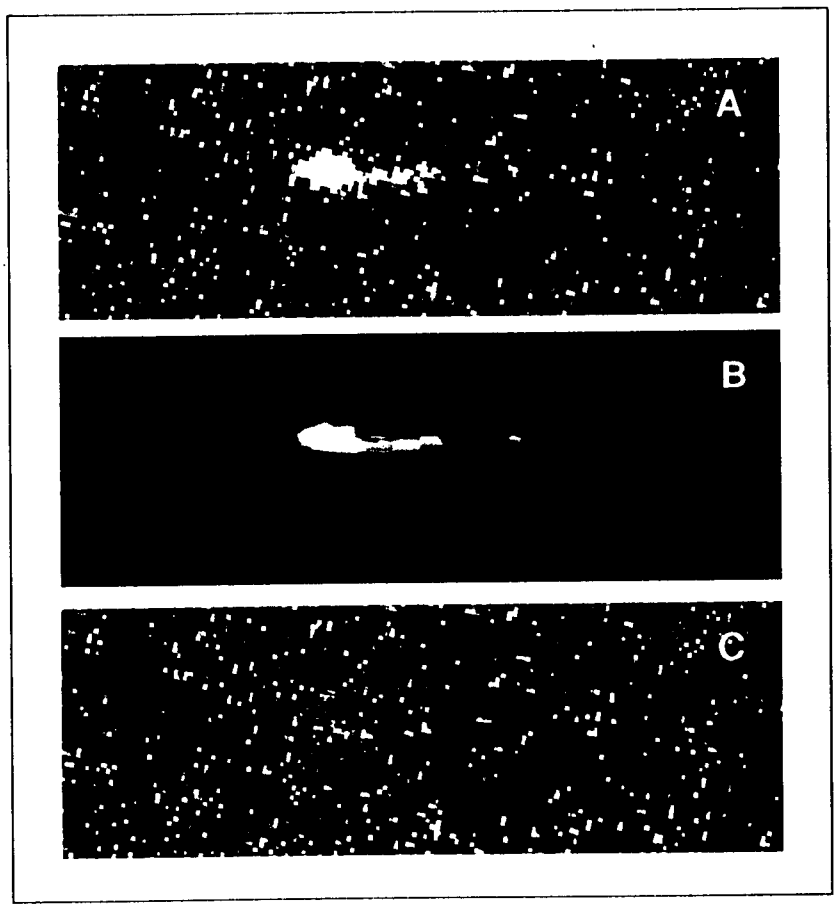

Trauger et al. Figure 3

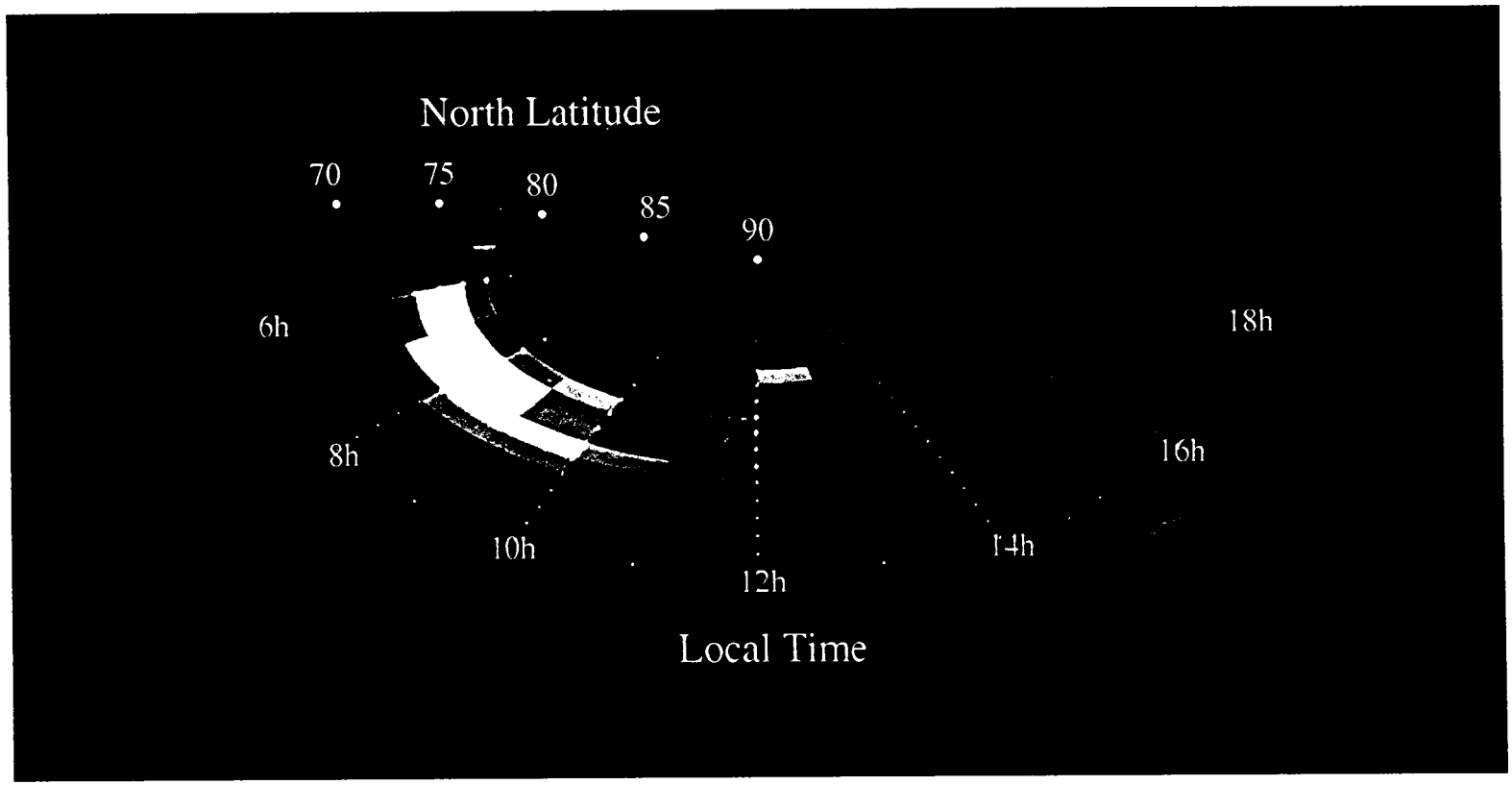

Trauger et al. Figure 4